Article:
Jacques, DA, Gooding, J, Giesekam, JJ et al. (2 more authors) (2014) Methodology for the assessment of PV capacity over a city region using low-resolution LiDAR data and application to the City of Leeds (UK). Applied Energy, 124. 28 - 34. ISSN 0306-2619

https://doi.org/10.1016/j.apenergy.2014.02.076

Methodology for the assessment of PV capacity over a city region using low-resolution LiDAR data and application to the City of Leeds (UK)

David A. Jacques, James Gooding, Jannik J. Giesekam, Alison S. Tomlin, Rolf Crook*

Energy Research Institute, School of Process, Environmental and Materials Engineering,

University of Leeds, LS2 9JT, United Kingdom.

* Corresponding author. Email address: R.Crook@leeds.ac.uk. Tel.: +44 113 34 37737

Abstract

An assessment of roof-mounted PV capacity over a local region can be accurately calculated by established roof segmentation algorithms using high-resolution light detection and ranging (LiDAR) datasets. However, over larger city regions often only low-resolution LiDAR data is available where such algorithms prove unreliable for small rooftops. A methodology optimised for low-resolution LiDAR datasets is presented, where small and large buildings are considered separately. The roof segmentation algorithm for small buildings, which are typically residential properties, assigns a roof profile to each building from a catalogue of common profiles after identifying LiDAR points within the building footprint. Large buildings, such as warehouses, offer a more diverse range of roof profiles but geometric features are generally large, so a direct approach is taken to segmentation where each LiDAR point within the building footprint contributes a separate roof segment. The methodology is demonstrated by application to the city region of Leeds, UK. Validation by comparison to aerial photography indicates that the assignment of an appropriate roof profile to a small building is correct in 81% of cases.

Keywords: PV capacity; PV output; LiDAR; Roof profile; Solar resource; City region

1. Introduction

Photovoltaics (PV) are viewed as a key climate change mitigation technology. To achieve this potential will require the large scale installation of PV, either on rooftops or as ground mounted arrays [1]. Installing highly distributed PV within city environments, such as on building rooftops and facades, locates electricity generation close to electricity end use, reducing the requirement for modifications to the electricity distribution network and minimizing transmission losses. Roof mounted PV also avoids the cost and competition for land, and the possible social and environmental impacts associated with large arrays of ground mounted panels [2]. An accurate assessment of the potential roof-mounted PV capacity in city regions is an essential component for establishing regional and national carbon reduction policies and informing investment decisions [3]. However, such assessments are not straightforward because of the range in size, orientation, pitch, and geometric complexity typically found in roof profiles.

Previously reported methods to calculate the potential PV capacity over a city region include image analysis of geometrically-corrected high-resolution aerial photography [4, 5], statistical approaches based on correlations between building class, population, and roof profile [6-8], and

roof profile reconstruction from light detection and ranging (LiDAR) point clouds [9-20]. Methods that utilise LiDAR data usually employ an error-minimising plane-fitting algorithm that divides each roof in to an arbitrary set of planes, which are referred to as roof segments. While such methods report high accuracy for large geometrically simple roofs, such as warehouses, they invariably require high-resolution LiDAR data to achieve accurate results for small buildings, such as residential properties, with inherently more complex roof profiles. This need for high-resolution data often arises from the use of data driven methods such as Hough transform, random sample consensus (RANSAC), or region growing based techniques [18-20]. The presence of trees, chimneys, aerials, and dormer windows can further reduce accuracy, compounded by errors in LiDAR location referencing, noise, and ranging artefacts.

This paper presents a methodology for the accurate reconstruction of roof profiles using low-resolution LiDAR data combined with building footprint datasets and knowledge of common roof profiles, recognising that using low-resolution LiDAR data alone is unlikely to generate accurate results. Compared to high-resolution LiDAR data, low-resolution data has greater coverage and is available at lower cost, making the methodology scalable to the regional and national level. A catalogue of common roof profiles is required, which is here localised for the UK. It is anticipated that application to other nations would require only a minor modification to the catalogue. The methodology is discussed is section 2 and applied to the city region of Leeds as a case study in section 3.

2. Methodology

The methodology is motivated by the need to accurately assess PV capacity over large regions of the built environment. The algorithms utilise low-resolution (2 m for the applied case study) LiDAR data, building footprint data, and knowledge of common roof profiles. Other information, such as knowledge of building types and their frequency over the region is not used because such data is not routinely available and is rarely provided in a common format. For each building a set of planar roof segments are generated, allowing the presentation of segment orientation and pitch histograms in addition to plots of specific energy yield and cumulative annual capacity.

A visual inspection of aerial photographs confirms that large rooftops, from a variety of commercial and civic buildings, are usually geometrically simple but exhibit a wide variety of profile forms. This is in contrast to small rooftops, from residential properties, which can be geometrically complex but conform to a small catalogue of profile forms. This motivates the division of rooftops into small and large based on building footprint area. The determination of what constitutes as small and large buildings will be location specific and can be determined based on cultural and architectural factors. The two divisions are then processed using different algorithms.

2.1 Small buildings

Most roof profiles for UK residential properties can be classified as gabled, hipped, or flat. A gabled profile consists of two flat segments intersecting along the roof ridge, while a hipped roof profile consist of four segments intersecting at 45° to the building sides when viewed from

above, as illustrated in figure 1. In all cases, every segment has the same pitch. These basic roof profiles can be adorned by chimneys, dormer windows, attached garages, porches, and extensions. A single rooftop can be shared by a number of properties. Terrace properties usually share a roof with a gabled profile, while semi-detached properties often share a roof with a hipped profile.

Each small building is considered in turn. LiDAR points that lie within the building footprint polygon are extracted from the LiDAR point cloud. This subset of LiDAR points is then rotated to both determine the orientation of the roof and prepare LiDAR point position data for roof profile classification. The centre point is defined as the point midway between the minimum and maximum LiDAR point positions in the x and y directions, where z is defined as elevation. The LiDAR points are rotated about the centre point in order to minimise the range of LiDAR point positions in the y direction, and the rotation angle is recorded as the roof orientation. This procedure identifies the minor axis, and it is assumed that the major axis lies perpendicular to this.

Each rooftop is then classified as either gabled, hipped, flat, complex, or unclassified, as illustrated in figure 1. Figure 2 plots sets of LiDAR points when viewed along the major axis of example buildings, illustrating each of the different roof profile classes. The roof edges are provided as a guide. The classification algorithm continues by dismissing LiDAR points with an elevation lower than 4 m below the building maximum elevation. Such points are typically associated with porches or garages, or result from location referencing errors in the LiDAR point cloud. If the number of LiDAR points is less than 10 then the algorithm proves inaccurate, so the rooftop is classed as unclassified. Further consideration is not required because such small buildings, owing to their small area are less appropriate for PV. The division into gabled or hipped uses linear regression to calculate best fit planes for assumed gabled and hipped profiles. These planes are the superposition of the roof segments rotated by 0°, 90°, 180°, or 270° as appropriate. The plane with the strongest correlation (highest Pearson product-moment correlation coefficient) to the LiDAR points determines the classification of the roof profile and the corresponding pitch of the roof. If the correlation is less than 0.4, then the roof is classed as complex. If the pitch of the roof is less than 15˚, then the roof is classed as flat. Employing this algorithm produces an appraisal of roof profiles and pitches across a wide study area more efficiently than other more complex statistical methods [21]. The roof profile classification algorithm is summarised below. Once a class has been established, the algorithm ends and the next building is considered.

1. Dismiss LiDAR points that are more than 4 m below the maximum elevation
2. Class as unclassified if there are fewer than 10 LiDAR points
3. Calculate the correlation to a best fit plane assuming a gabled profile
4. Calculate the correlation to a best fit plane assuming a hipped profile
5. Class as complex if the maximum correlation is less than 0.4
6. Class as flat if the pitch of the best correlation is less than 15°
7. Class as gabled or hipped as associated by the maximum correlation

The roof profile class then determines the area and orientation of roof space available for PV installation. For rooftops classed as gabled, the roof is split into two segments along a line

parallel to the major axis that passes through the centre point. The resource potential of the two segments are subsequently considered separately. For rooftops classed as hipped, the roof is split into four segments, and all segments are considered separately. Rooftops classed as flat have one available segment, with PV assumed to be supported by an angle mounting with 15° pitch facing due south. Rooftops classed as unclassified contribute zero PV capacity. For rooftops classed as complex, there is no guarantee that the calculated orientation or pitch will correspond to a large roof segment. It is likely that there will be multiple roof segments at various angles, so complex buildings are considered to be inappropriate for PV installation. For all segments, an area reduction factor takes in to account obstructions to PV installation including aerials, chimneys, dormer windows, and shading of the installation through artefacts such as vegetation and other buildings [7, 8, 22].

2.2 Large buildings

Large buildings exhibit a diverse range of roof profiles, so the catalogue based approach utilised for small buildings is not effective. However, geometric features on large building rooftops are generally larger than the spatial resolution of the LiDAR data, so a more direct approach can be taken to roof segmentation. The algorithm used here is similar to that used by ESRI ArcGIS [23].

Each large building is analysed in turn. The LiDAR points located within the building footprint polygon are then considered sequentially. Neighbouring LiDAR points are identified as those points that lie within a distance $(0.25 + 2^{0.5})d$ from the processed LiDAR point, where d is the spacing between LiDAR points. The LiDAR points are generally equally spaced within an orthogonal square grid, but are not always well orientated in the north-south east-west directions. By adding a buffer region to account for this, the equation ensures that all 9 nearest neighbours are found. For example, if the spacing between LiDAR points was 2 m, all points within a circle of radius 3.3 m will be found. This set of 9 local LiDAR points constitutes a 3 × 3 square array from which a roof segment pitch and orientation are calculated. If the set contains fewer than 9 points, then the processed LiDAR point must be close to the building boundary and is deemed unsuitable for PV installation.

A roof segment of area d^2 is associated with each LiDAR point. The best-fit plane to the set of 9 local LiDAR points is calculated using a least squares algorithm, providing dx, dy, and dz. The orientation of the segment is then calculated using Eq. (1),

$$orientation = \frac{360}{2\pi}\text{atan}_{4q}\left(\frac{dz}{dy}, -\frac{dz}{dx}\right) \quad (1)$$

where atan_{4q} is the 4-quadrant inverse tangent, and pitch is calculated using Eq. (2),

$$pitch = \frac{360}{2\pi}\text{atan}\left(\sqrt{\left(\frac{dz}{dy}\right)^2 + \left(\frac{dz}{dx}\right)^2}\right). \quad (2)$$

Some roof segments are distorted by location referencing errors in the LiDAR point cloud, or by roof furniture such as heating, ventilation, and air conditioning (HVAC) systems. Such segments are identified as having a pitch greater than 60°. These segments are dismissed, being either

erroneous or unsuitable for PV installation. The large building algorithm can be extended by grouping adjacent segments when they have similar orientation and pitch [24]. This would lead to improved efficiency when further analysing the roof segment dataset but does not improve accuracy.

3. Application to the city region of Leeds (UK)

The potential PV generation capacity was assessed over the city region of Leeds (UK) in order to demonstrate and validate the methodology. Leeds is a large city located in the north of England hosting a variety of domestic, commercial, and civic buildings of different ages and styles. The boundary of the region considered is identified in figure 3, which covers an area of 204 km^2 and includes 60,000 small buildings, which for the purpose of this case study are defined as having a footprint less than 200 m^2, and 15,000 large buildings. The population within this boundary is approximately 750,000 representing 1.2% of the UK population in 2011. Low-resolution LiDAR data was obtained from Landmap [25] with a grid resolution of 2 m and an elevation error margin of 0.15 m. There are 48×10^6 LiDAR points within the boundary. Building footprint data was obtained from Digimap [26]. The LiDAR points lying within each building footprint were filtered using a GIS-based system with output datasets in a text-based format. This resulted in a total of 5×10^6 LiDAR points under consideration. The total rooftop area available in the assessed region is 5.0×10^6 m^2 on small buildings and 11.3×10^6 m^2 on large buildings. Subsequent analysis was performed using MATLAB [27] running on a desktop computer. The assessment took 24 minutes, averaging 0.01 seconds for a building. To take into account shading and other roof uses, an area reduction factor of 0.9 was applied, following previous literature appropriate for Europe [28].

3.1 Roof profile assessment

Figure 4 shows frequency histograms for the orientation and pitch of roof segments weighted by the segment area. Data for small and large buildings is considered both separately and combined. With reference to figure 4a, the pitch of rooftops on small buildings peaks at 30° with the vast majority of small buildings having pitches within 10° of this value. A small peak at 15° occurs because flat roofs are assigned an angle of 15° for mounting PV. Figure 4b indicates that there are two common pitches for large buildings, one at 0° for flat roofs, and one at 9° which corresponds to the common 2:12 design accommodating efficient water run-off. Above 40° the frequency drops sharply for small buildings, but figure 4b exhibits a long tail which is consistent with the more varied range of rooftop designs and features seen in larger buildings.

With reference to figure 4d, there is no clear preference for the orientation of small buildings. A 180° rotational symmetry is observed. This is because every roof segment has an associated opposite segment on the same rooftop, resulting from the geometrically symmetric nature of the roof profile classes. However, figure 4e reveals that large buildings do have a preference for southerly orientation, making them particularly well suited for PV installation. This does not appear to be influenced by the orientation of roads or rivers, or the landscape topography of the region. Note that the algorithm used to establish the orientation of small buildings results in some angular quantisation inherent from the orthogonal nature of the LiDAR point cloud and small size of the buildings. Hence, a minimum bin size of 45° is necessary in figures 4d and 4f to

generate accurate histograms. For the same reason, small building orientation has a maximum error of ±22.5° becoming smaller with larger rooftops. However, this has little impact on the annual output because insolation is relatively insensitive to orientation changes less than 22.5°. Furthermore, for regional calculations where many rooftops are considered collectively these random errors will tend to cancel.

The cumulative annual output of the city region of Leeds was calculated using the online PVGIS tool provided by the European Commission Joint Research Centre [29, 30]. The variables were set as latitude of 53°48'4" north, longitude of 1°32'54" west, CMSAF database, with an assumed system efficiency of 15%. The optimal pitch for the installation of PV at this location is 39°. A matrix of generation output data was calculated based on PVGIS with a 6° resolution in pitch and a 10° resolution in orientation. A performance factor was then assigned to each roof segment based on orientation and pitch, using linear interpolation between the tabulated values. Figure 5 shows specific annual yield and cumulative annual output plotted against the fraction of the total rooftop area available for PV. Small and large buildings were considered separately and combined. The most optimally angled roof segments are considered first, so the specific annual yield decreases and the cumulative annual output curve exhibits a decreasing gradient as less optimal segments contribute less to the total generation. Small buildings exhibit a higher specific annual yield compared to large buildings. This is because the pitch of small buildings is generally closer to the optimal value.

The changes in gradient of the output curves are less accentuated than might be expected given that a vertical north-facing roof segment provides an annual output approximately 25% of that from an optimally angled segment [26, 27]. The output curves do reach this reduced gradient when the fraction of area is equal to one. However, the number of roof segments with extremely poor orientation and pitch is negligible and not visible on the output curves. In the case of small buildings, the output curves are dominated by rooftops with a pitch of approximately 30°. In this case, the annual output from a north facing segment is approximately 60% of that from a south facing segment.

3.2 Validation

The small building roof profile classification algorithm was validated using a random sample of 242 buildings from the city region of Leeds. Each building was classified using both the algorithm described here and visually using geometrically-corrected aerial photographs. Table 1 shows the coincidence of this comparison. The random selection gave a fair representation of the ratio of the frequency of the different building types confirming that it is indeed a reliable sample.

Table 1 highlights the success of the algorithm at identifying hipped rooftops, yet 18% of gabled rooftops were incorrectly classified as hipped. The algorithm is poor at identifying all complex rooftops. However, complex rooftops occur infrequently so this has a minimal impact on cumulative annual output calculations. Errors in roof profile classification are likely to be caused by elevation or location referencing errors associated with the LiDAR dataset, angular quantisation errors, or the presence of dormer windows or chimneys coinciding with LiDAR data points. The overall success rate, using low-resolution LiDAR data, is 81%.

It is informative to consider the performance of alternative algorithms, which were originally designed for use with higher resolution LiDAR datasets, now implemented with low-resolution data. Triangular irregular networks (TINs) are often generated from LiDAR point clouds as part of an algorithm to generate roof profiles [14-17]. Figure 6 provides a comparison of the small building algorithm output against aerial photographs, TIN profiles, and the large building algorithm output, all utilising the same low-resolution data. The TIN roof profiles provide a poor rooftop representation. Using the large building algorithm, a histogram of the pitches of generated segments is shown. The number of different pitches and their values are unrealistic.

4. Conclusion

A computationally efficient methodology for roof profile classification is presented, for the purpose of regional PV capacity assessment, using widely available low-resolution LiDAR datasets. In this methodology, small and large buildings are considered separately. The roof segmentation algorithm for small buildings assigns a roof profile to each building from a catalogue of common profiles after identifying LiDAR points within the building footprint. Large buildings offer a more diverse range of roof profiles but geometric features are generally large, so a direct approach is taken to segmentation where each LiDAR point contributes a separate segment. The methodology was demonstrated by application to the city region of Leeds, UK, with 75,000 buildings. Validation by comparison to aerial photography indicates that the assignment of an appropriate roof profile to a small building is correct in 81% of cases. The small building algorithm also compares well against other methods that typically require higher resolution data such as TIN algorithms. The methodology is readily scalable for county or national assessment of potential PV capacity. It is anticipated that application to other nations would require only a minor modification to the roof profile catalogue. An accurate dataset of roof-mounted PV capacity over city regions can assist strategic planning for carbon reduction by, for example, the identification of optimal locations for cost effective PV installations or assessment of the impact of regional policy change. With data values for every building in a city region, the dataset could be coupled with an interactive mapping tool to inform residents of individual building PV capacity.

Acknowledgements

This work was financially supported by the Engineering and Physical Sciences Research Council through the University of Leeds Doctoral Training Centre in Low Carbon Technologies.

References

[1] DECC. The Carbon Plan: Delivering our low carbon future, Annex A,. 2011.
[2] Chiabrando R, Fabrizio E, Garnero G. The territorial and landscape impacts of photovoltaic systems: Definition of impacts and assessment of the glare risk. Renewable and Sustainable Energy Reviews. 2009;13:2441-51.
[3] Hay JE, Hanson KJ. Evaluating the solar resource: a review of problems resulting from temporal, spatial and angular variations. Solar Energy. 1985;34:151-61.

[4] Bergamasco L, Asinari P. Scalable methodology for the photovoltaic solar energy potential assessment based on available roof surface area: Further improvements by ortho-image analysis and application to Turin (Italy). Solar Energy. 2011;85:2741-56.
[5] Kabir MH, Endlicher W, Jägermeyr J. Calculation of bright roof-tops for solar PV applications in Dhaka Megacity, Bangladesh. Renewable Energy. 2010;35:1760-4.
[6] Brito MC, Gomes N, Santos T, Tenedório JA. Photovoltaic potential in a Lisbon suburb using LiDAR data. Solar Energy. 2012;86:283-8.
[7] Izquierdo S, Rodrigues M, Fueyo N. A method for estimating the geographical distribution of the available roof surface area for large-scale photovoltaic energy-potential evaluations. Solar Energy. 2008;82:929-39.
[8] Wiginton LK, Nguyen HT, Pearce JM. Quantifying rooftop solar photovoltaic potential for regional renewable energy policy. Computers, Environment and Urban Systems. 2010;34:345-57.
[9] Gooding J, Edwards H, Giesekam J, Crook R. Solar City Indicator: A Methodology to Predict City Level PV Installation Capacity by Combining Physical Capacity and Socio-economic Factors. Solar Energy. 2013;95:325-35.
[10] Kassner R, Koppe W, Schüttenberg T, Bareth G. Analysis of the solar potential of roofs by using official lidar data. International Archives of Photogrammetry, Remote Sensing and Spatial Information Sciences. 2008;37:399-403.
[11] Jochem A, Höfle B, Rutzinger M, Pfeifer N. Automatic Roof Plane Detection and Analysis in Airborne Lidar Point Clouds for Solar Potential Assessment. Sensors. 2009;9:5241-62.
[12] Kodysh JB, Omitaomu OA, Bhaduri BL, Neish BS. Methodology for estimating solar potential on multiple building rooftops for photovoltaic systems. Sustainable Cities and Society. 2013;8:31-41.
[13] Lukač N, Žalik B. GPU-based roofs' solar potential estimation using LiDAR data. Computers & Geosciences. 2013;52:34-41.
[14] Nguyen HT, Pearce JM, Harrap R, Barber G. The Application of LiDAR to Assessment of Rooftop Solar Photovoltaic Deployment Potential in a Municipal District Unit. Sensors. 2012;12:4534-58.
[15] Vosselman G, Dijkman S. 3D building model reconstruction from point clouds and ground plans. International Archives of the Photogrammetry, Remote Sensing and Spatial Information Sciences. 2001;34:37-44.
[16] Awwad TM, Zhu Q, Du Z, Zhang Y. An improved segmentation approach for planar surfaces from unstructured 3D point clouds. Photogramm. Rec. 2010;25:5-23.
[17] Gorte B. Segmentation of TIN-structured surface models. International Archives of the Photogrammetry, Remote Sensing and Spatial Information Sciences. 2002;34(4):465-469.
[18] Nguyen V, Martinelli A, Tomatis N, Siegwart R. A comparison of line extraction algorithms using 2D laser rangefinder for indoor mobile robotics. IEEE/RSJ International Conference: IEEE; 2005. p. 1929-34.
[19] Overby J, Bodum L, Kjems E, Iisoe P. Automatic 3D building reconstruction from airborne laser scanning and cadastral data using Hough transform. International Archives of Photogrammetry and Remote Sensing. 2004;35:296-301.
[20] Rottensteiner F, Trinder J, Clode S, Kubik K. Automated delineation of roof planes from lidar data. International archives of the photogrammetry, remote sensing and spatial information sciences. 2005;36:221-6.

[21] Maas H-G. Closed solutions for the determination of parametric building models from invariant moments of airborne laserscanner data. transformation. 1999;2:20.
[22] Pillai IR, Banerjee R. Methodology for estimation of potential for solar water heating in a target area. Solar Energy. 2007;81:162-72.
[23] Burrough PA, McDonnell RA. Principles of geographical Information Systems: Oxford University Press; 1998.
[24] Rottensteiner F, Briese C. Automatic generation of building models from LIDAR data and the integration of aerial images. International Archives of the Photogrammetry, Remote Sensing and Spatial Information Sciences of the ISPRS. 2003;34:174-80.
[25] Cities Revealed © The GeoInformation Group. 2008.
[26] OS MasterMap [Shape geospatial data], Updated: December 2011, Ordnance Survey (GB), Using: EDINA Digimap Ordnance Survey Service, <http://edina.ac.uk/digimap>, Downloaded: February 2013
[27] MATLAB. R2012a. Natick, Massachusetts.
[28] Lehmann H, Peter S. Assessment of roof & façade potentials for solar use in Europe. Institute for sustainable solutions and innovations (ISUSI): Aachen, Germany. 2003.
[29] Huld T, Müller R, Gambardella A. A new solar radiation database for estimating PV performance in Europe and Africa. Solar Energy. 2012;86:1803-15.
[30] Šúri M, Huld TA, Dunlop ED, Ossenbrink HA. Potential of solar electricity generation in the European Union member states and candidate countries. Solar Energy. 2007;81:1295-305.

		Validation by aerial photography					
		Gabled	Hipped	Flat	Complex	Unclassified	
Classification using algorithm	Gabled	**74**	7	0	1	0	82
	Hipped	18	**111**	2	3	0	134
	Flat	0	0	**3**	2	0	5
	Complex	5	6	0	**5**	0	16
	Unclassified	0	0	0	0	**5**	5
		97	124	5	11	5	242

Table 1: Comparison between classification from algorithm and validation from aerial photography. The units are number of buildings.

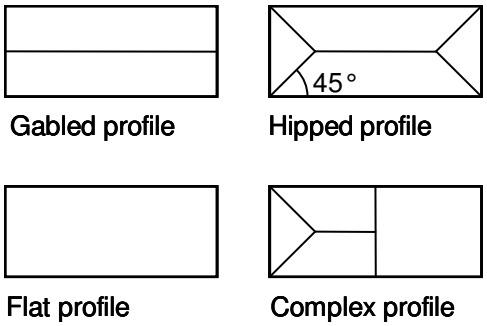

Figure 1: Illustration of roof profile catalogue when viewed from above. Depiction of a complex profile is an example.

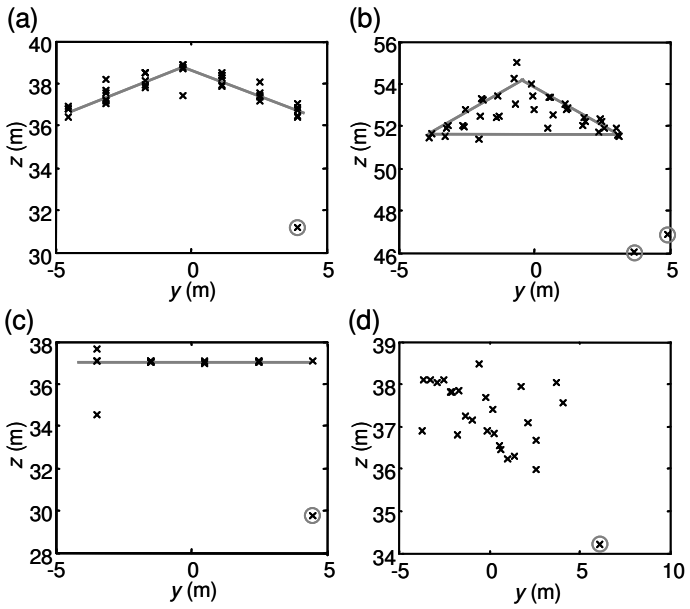

Figure 2: Sets of typical LiDAR points to illustrate each of the roof profile classes: a) gabled, b) hipped, c) flat, and d) complex. Points are viewed along the major axis. Grey lines provide a guide to the profile. Grey circles identify LiDAR points that are dismissed.

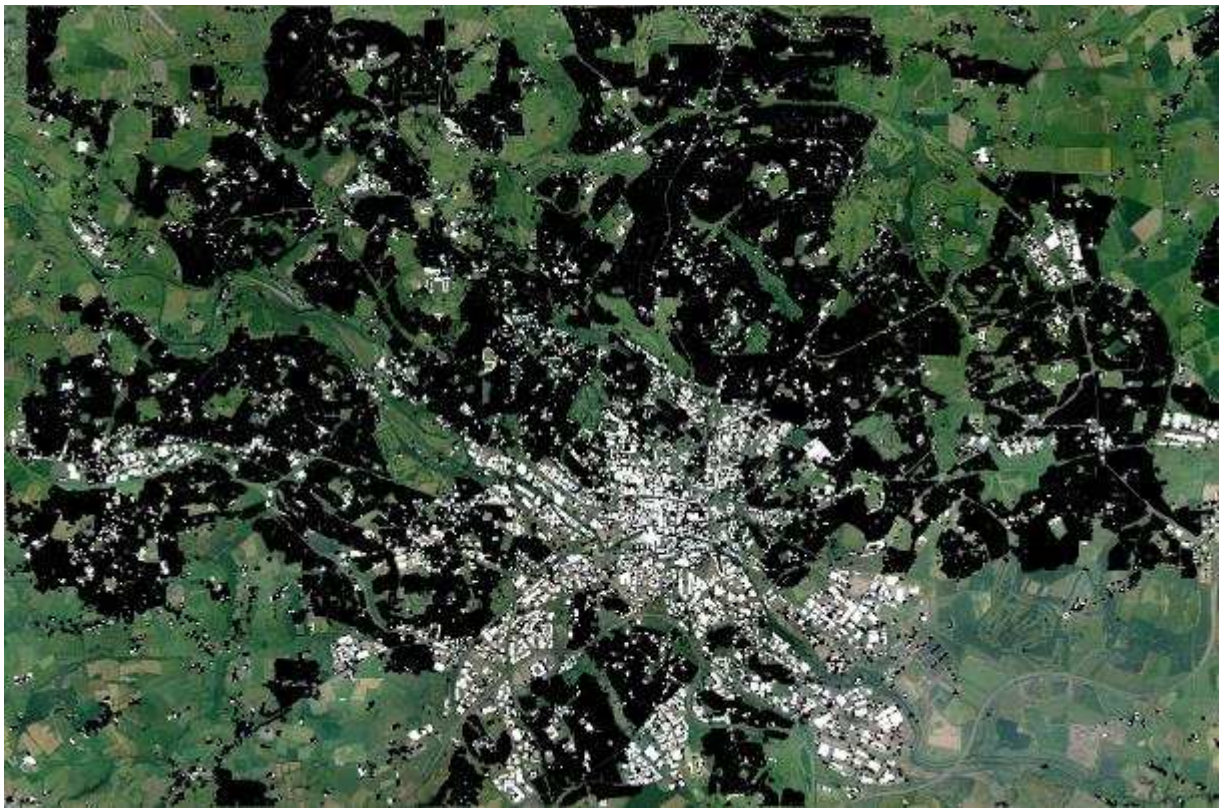

Figure 3: Boundary of the City of Leeds used in this assessment. Geometrically-corrected aerial photograph overlaid with small and large buildings filled in black and white respectively. Credit for photography: UKMap © The GeoInformation Group 2006; OS MasterMap [Shape geospatial data] EDINA Digimap Ordnance Survey Service 2013.

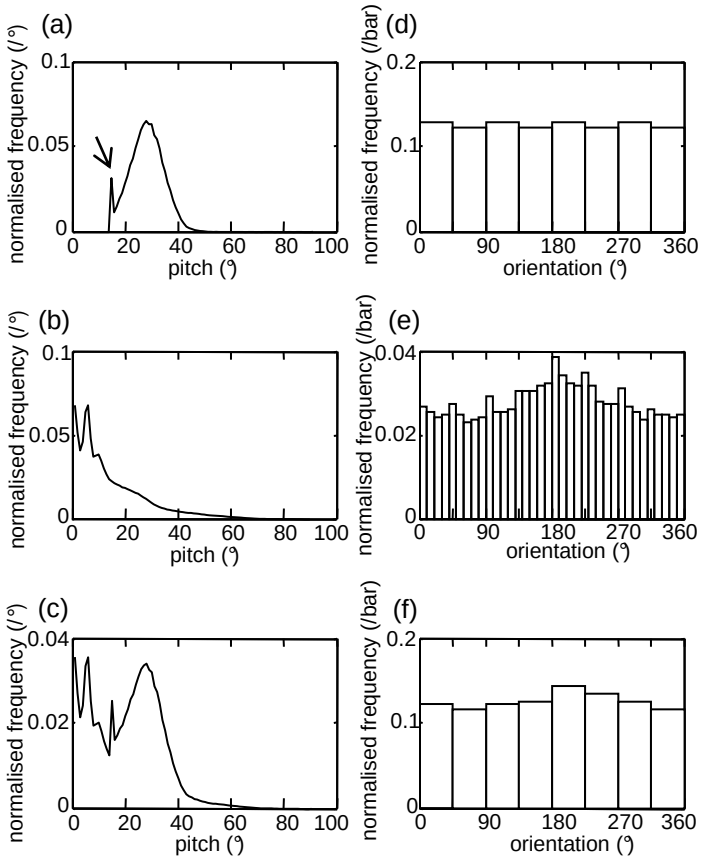

Figure 4: Area weighted histograms of roof segments for a) pitch of small buildings, b) pitch of large buildings, c) pitch of all buildings, d) orientation of small buildings, e) orientation of large buildings, and f) orientation of all buildings. Roof pitches are plotted as angles relative to the horizontal. Orientations are plotted as angles relative to north in a clockwise direction. The arrow in plot a) indicates the effect of assigning a pitch of 15° to all flat roofs.

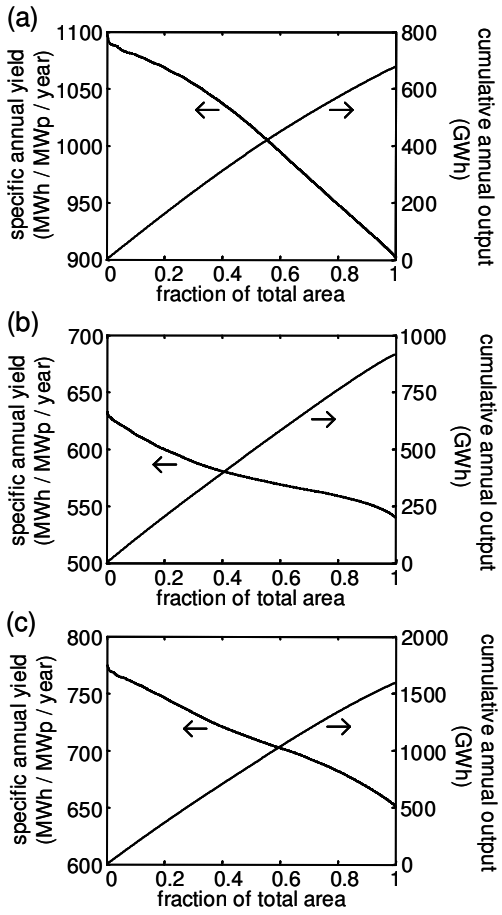

Figure 5: Plots of specific annual yield and cumulative annual output as a function of fraction of total area for a) small buildings, b) large buildings, and c) all buildings. The most optimally angled roof segments are considered first.

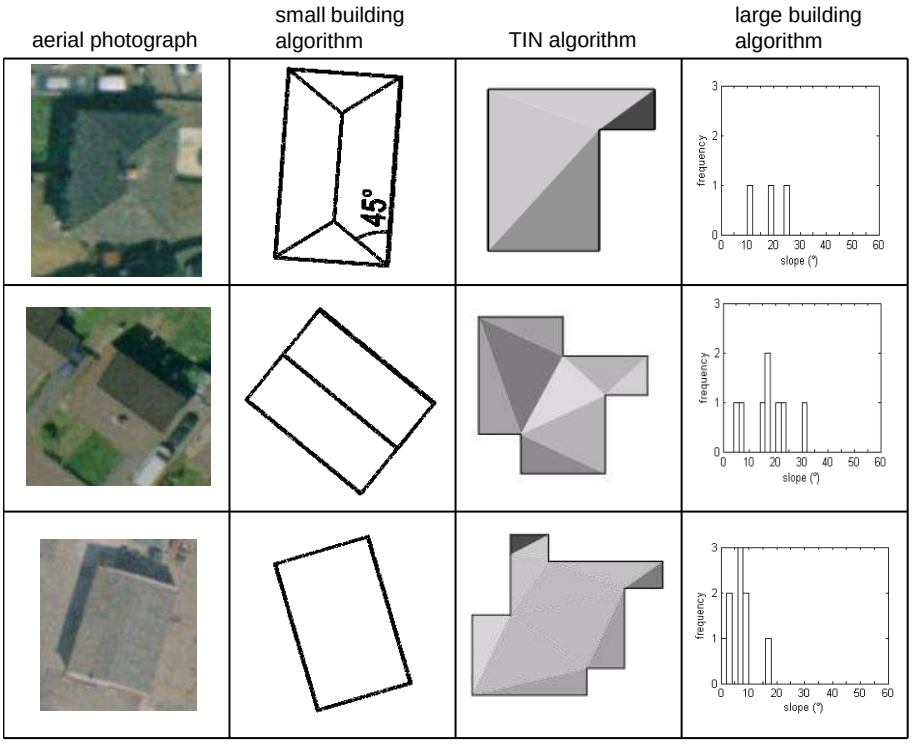

Figure 6: Comparison of the small building algorithm output, the TIN algorithm output, and the large building algorithm output, for examples of respectively small building hipped, gabled, and flat roof profiles. Credit for photography: UKMap © The GeoInformation Group 2006; OS MasterMap